THE JOURNAL OF PHYSICAL CHEMISTRY A

Article

Cite This: J. Phys. Chem. A 2019, 123, 3703−3708

pubs.acs.org/JPCA

# Structures and Infrared Spectra of $[M(CO_2)_7]^+$ (M = V, Cr, and Mn) Complexes

Dong Yang,[†,‡,§] Xiangtao Kong,[†,§] Huijun Zheng,[†,‡] Mingzhi Su,[†,‡] Zhi Zhao,[†] Hua Xie,[†] Hongjun Fan,[†] Weiqing Zhang,[†] and Ling Jiang*[,†]

[†]State Key Laboratory of Molecular Reaction Dynamics, Collaborative Innovation Center of Chemistry for Energy and Materials (iChEM), Dalian Institute of Chemical Physics, Chinese Academy of Sciences, 457 Zhongshan Road, Dalian 116023, China

[‡]University of Chinese Academy of Sciences, 19A Yuquan Road, Beijing 100049, China

Supporting Information

**ABSTRACT:** Gas-phase infrared photodissociation spectra of $[V(CO_2)_n]^+$ complexes revealed three new vibrational bands at 1140, 1800, and 3008 $cm^{-1}$ at $n = 7$, the features of which are retained in the larger clusters (Ricks, A. M.; Brathwaite, A. D.; Duncan, M. A. *J. Phys. Chem. A* **2013,** *117,* 11490−11498). However, structural assignment of this intriguing feature remains open. Herein, quantum chemical calculations on $[V(CO_2)_7]^+$ were carried out to identify the structure of the low-lying isomers and to assign the observed spectral features. The comparison of calculated infrared spectra of $[V(CO_2)_7]^+$ with experimental infrared spectra identified the formation of a bent $CO_2^-$ species, suggesting the ligand-induced activation of $CO_2$ by the vanadium cation. The structures and infrared spectra of $[Cr(CO_2)_7]^+$ and $[Mn(CO_2)_7]^+$ were also predicted and discussed.

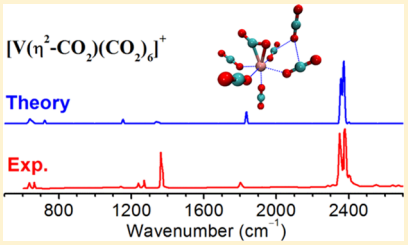


## 1. INTRODUCTION

Transformation of carbon dioxide into chemical products of value has received increasing attention over the past decades.[1,2] Transition-metal catalysts are widely used for these processes. Vibrational spectroscopic signatures of molecular level mechanics are often masked by the diffuse nature of the key bands in the condensed phase. Cluster spectroscopy coupled with mass spectrometry in the gas phase can mass-select the complexes of interest and analyze them without the interference of the surrounding environment, which provides the structural and spectral information for mechanistic understanding of a chemical reaction.[3−6]

The interaction of $CO_2$ with the excess electron leads to a deformation of the $CO_2$ molecule from the linear geometry of the neutral to a bent anion. The O−C−O bond angle of $CO_2^-$ anion species has been determined by a variety of experimental[7−10] and theoretical[11,12] methods to be about 134°. Gas-phase infrared photon dissociation spectroscopic studies on the mass-selected metal anion−$CO_2$ complexes have characterized the monodentate coordination $[M(\eta^1\text{-}CO_2)]^-$ for $Cu^-$, $Ag^-$, $Au^-$, and $Bi^-$ anions[13−16] and the bidentate coordination $[M(\eta^2\text{-}CO_2)]^-$ for $Co^-$ and $Ni^-$ anions.[17,18] Switching from monodentate coordination $[M(\eta^1\text{-}CO_2)]^-$ to oxalate species $[M(C_2O_4)]^-$ was observed in the $[Bi(CO_2)_n]^-$ complexes.[13] Gas-phase infrared photodissociation (IRPD) spectroscopy of $[ClMg(\eta^2\text{-}O_2C)]^-$ revealed a bidentate double oxygen metal−$CO_2$ coordination fashion.[19] The $\eta^2$-$CO_2$, $\eta^2$-oxalate, and oxide-carbonyl motifs have been observed in the anionic $[M(CO_2)_n]^-$ (M = Fe and Ti) complexes.[20,21] The reactivity of cobalt cluster anions $Co_n^-$ ($n$ = 3−17) toward dissociative activation of $CO_2$ occurs at $n = 7$, peaks at $n$ = 8−10, and then gradually decreases with increasing cluster size.[22] Interestingly, dissociative activation of $CO_2$ emerges on the $Pt_n^-$ clusters with $n \geq 5$.[23]

In general, the $CO_2$ molecule is weakly bound to the metal cations in an "end-on" configuration via electrostatic interactions ($\eta^1$-OCO), as exemplified by IRPD spectroscopy of $[M(CO_2)_n]^+$ (M = Fe, Al, Co, Rh, Ir, Cu, and Ag) complexes.[24−27] Gas-phase kinetics studies have shown that only nine atomic metal cations ($Sc^+$, $Ti^+$, $Y^+$, $Zr^+$, $Nb^+$, $La^+$, $Hf^+$, $Ta^+$, and $W^+$) are able to reduce $CO_2$ to form the oxide-carbonyl structure $[OMCO]^+$ at room temperature.[28] IRPD spectroscopy of $[Ti(CO_2)_2Ar]^+$ and $[Ti(CO_2)_n]^+$ ($n$ = 3−7) indicated that there was a sharp band in the CO stretching vibration region, suggesting that $Ti^+$ is able to reduce $CO_2$ to form the oxide-carbonyl structure $[OTiCO]^+$.[29] The oxide-carbonyl complexes $[OMCO(CO_2)_{n-1}]^+$ have been observed for $Ni^+$ and $Si^+$.[30,31]

Interestingly, recent IRPD spectroscopy of reaction of $V^+$ with $CO_2$ by adding one $CO_2$ molecule at a time revealed that the $CO_2$ molecules are weakly coordinated to the metal in the $n \leq 6$ clusters. Three new vibrations of 1140, 1800, and 3008 $cm^{-1}$ were observed at $n = 7$, the features of which were retained in the larger clusters.[32] The formation of an oxalate-type $C_2O_4^-$ anion species was proposed to account for these intriguing observations. However, the conclusive identification of the cluster structure remains open. In this work, quantum chemical calculations on $[V(CO_2)_7]^+$ were carried out to identify the structure of the low-lying isomers and to assign the observed spectral features. Considering that Cr and Mn are

**Received:** January 2, 2019
**Revised:** April 7, 2019
**Published:** April 8, 2019






DOI: 10.1021/acs.jpca.9b00041
J. Phys. Chem. A 2019, 123, 3703−3708

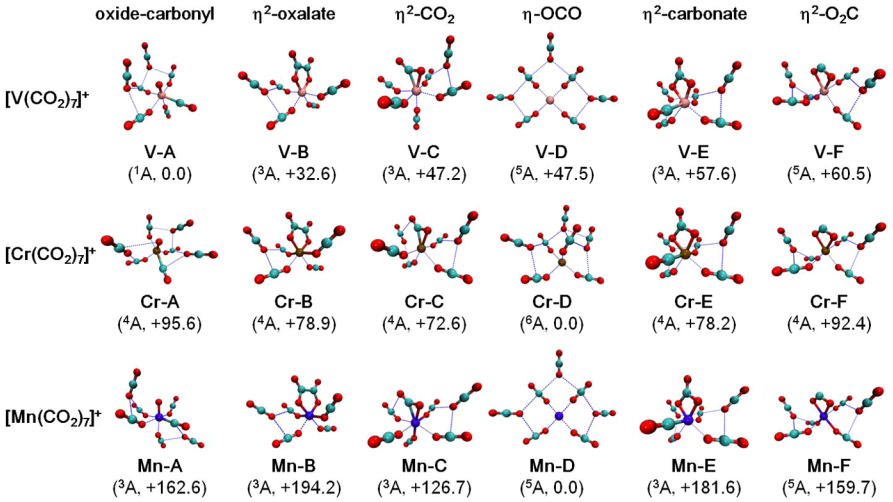


**Figure 1.** Optimized structures of $[M(CO_2)_n]^+$ (M = V, Cr, Mn) (O, red; C, cyan; V, pink; Cr, ochre; Mn, violet). Relative energies (inside brackets) are given in kJ/mol.

close to V in the series of 3d transition-metal cations, the structure and infrared spectra of $[Cr(CO_2)_7]^+$ and $[Mn(CO_2)_7]^+$ were also calculated and compared to those of $[V(CO_2)_7]^+$. The comparison of calculated IR spectra of $[V(CO_2)_7]^+$ with experimental IR spectra reveal the formation of a bent $CO_2^-$ species, suggesting the ligand-induced activation of $CO_2$ by the vanadium cation.

## 2. COMPUTATIONAL METHOD

Quantum chemical calculations were performed using the Gaussian 09 program.[33] The B3LYP hybrid functional augmented with a dispersion correction (B3LYP-D3) was utilized. The def2-TZVPP basis set was used for the V, Cr, Mn, C, and O atoms. Different metal−$CO_2$ coordination modes discussed in the literature[3,4,6,19,34] were calculated for the $[M(CO_2)_7]^+$ (M = V, Cr, and Mn) cation, resulting in six structural motifs (i.e., oxide-carbonyl, $\eta^2$-oxalate, $\eta^2$-$CO_2$, $\eta^1$-OCO, $\eta^2$-carbonate, and $\eta^2$-$O_2C$) (see Figure 1), where superscripts denote the number of bonds between the metal atom and the $CO_2$ ligand and chemical element symbols describe the atoms directly interacting with the metal. Possible spin states were considered. Relative energies and binding energies included zero-point vibrational energies. Harmonic vibrational frequencies were scaled by a factor of 0.9752 to account for the systematic errors,[13] which were determined by a comparison of experimental and calculated frequencies of the free $CO_2$ molecule. The resulting stick spectra were convoluted by a Gaussian line-shape function with a full width at half maximum linewidth of 10 $cm^{-1}$, in order to account for line-broadening effects.

The EDA-NOCV analysis (energy decomposition analysis-natural orbitals for chemical valence)[35] was performed with ADF2018[36−38] using the functional BP86-D3(BJ) level and the triple-$\zeta$ with double polarization function Slater-type orbitals as basis sets for the self-consistent field calculations. The interaction energy ($\Delta E_{int}$) between two fragments is decomposed into four energy terms, viz., the electrostatic interaction energy ($\Delta E_{elstat}$), the Pauli repulsion ($\Delta E_{Pauli}$), the orbital interaction energy ($\Delta E_{orb}$), and the dispersion interaction energy ($\Delta E_{disp}$), Therefore, the interaction energy ($\Delta E_{int}$) between two fragments can be defined as

$$\Delta E_{int} = \Delta E_{elstat} + \Delta E_{Pauli} + \Delta E_{orb} + \Delta E_{disp}$$

## 3. RESULTS AND DISCUSSION

Optimized structures of $[M(CO_2)_n]^+$ (M = V, Cr, and Mn) are illustrated in Figure 1. Representatively, relative energies of the isomers with different spin states for $[V(CO_2)_7]^+$ are given in Table S1. The comparison of the experimental IRPD spectrum to the calculated IR spectra for $[V(CO_2)_7]^+$ is shown in Figure 2 and band assignments are listed in Table 1. The calculated IR spectra of $[Cr(CO_2)_7]^+$ and $[Mn(CO_2)_7]^+$ are depicted in Figures 3 and 4, respectively.

**3.1. $[V(CO_2)_7]^+$.** As shown in Figure 1, the lowest-energy isomer for $[V(CO_2)_7]^+$ (labeled **V-A**) consists of an oxide-carbonyl structure $[OVCO(CO_2)_6]^+$ with a $^1A$ state, in which three $CO_2$ molecules are bound directly to the metal in the first-coordination shell and three $CO_2$ molecules are weakly

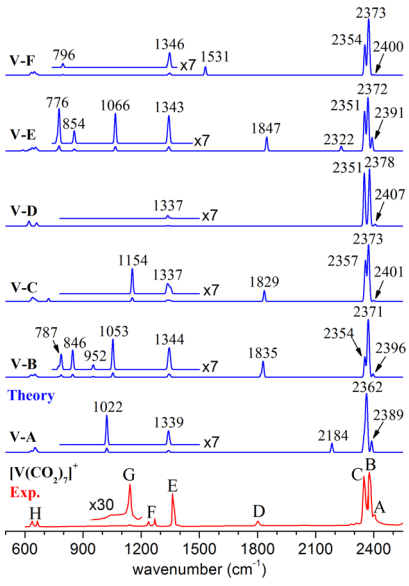


**Figure 2.** Comparison of the experimental IRPD spectrum of $[V(CO_2)_7]^+$ to the calculated IR spectra of the six lowest-energy isomers. The experimental spectrum was digitized from the literature.[32]



DOI: 10.1021/acs.jpca.9b00041
J. Phys. Chem. A 2019, 123, 3703−3708

**Table 1. Experimental Band Positions ($cm^{-1}$) of $[V(CO_2)_7]^+$ and Calculated Harmonic Frequencies ($cm^{-1}$) and Band Assignments of the V-C Isomer**

| label | Exp. | V-C | assignment |
|---|---|---|---|
| A | 2402 | 2401 | in-phase combinations of $CO_2$ antisymmetric stretch |
| B | 2376 | 2373 | out-of-phase combinations of $CO_2$ antisymmetric stretch |
| C | 2348 | 2357 | antisymmetric stretch of the second-sphere $CO_2$ |
| D | 1800 | 1829 | C═O antisymmetric stretch of $CO_2^-$ |
| E | 1363 | 1337 | $CO_2$ symmetric stretch |
| F | 1267 | | overtone of bending mode of the second-sphere $CO_2$ |
| | 1237 | | overtone of bending mode of the first-sphere $CO_2$ |
| G | 1140 | 1154 | C═O symmetric stretch of $CO_2^-$ |
| H | 664 | 721 | bending mode of the second-sphere $CO_2$ |
| | 637 | 639 | bending mode of the first-sphere $CO_2$ |

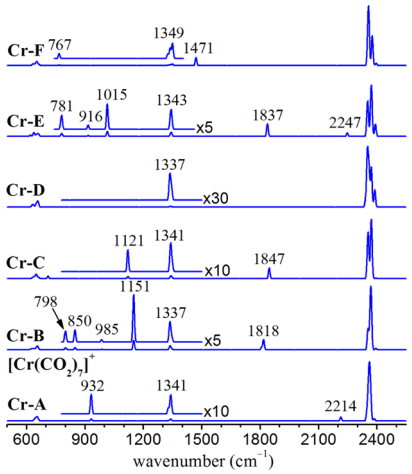


**Figure 3.** Simulated IR spectra of the six lowest-energy isomers for $[Cr(CO_2)_7]^+$.

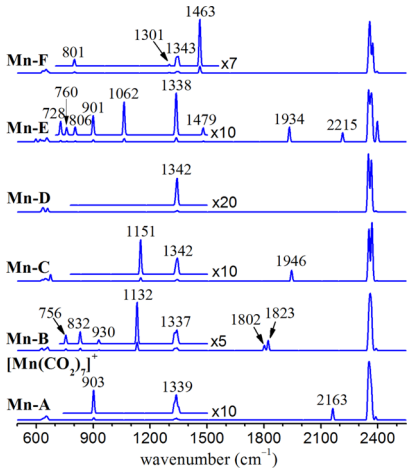


**Figure 4.** Simulated IR spectra of the six lowest-energy isomers for $[Mn(CO_2)_7]^+$.

tagged in the second-coordination shell. The next energetically higher isomer (**V-B**, +32.6 kJ/mol) has an $\eta^2$-oxalate ion core. In the third isomer, **V-C**, a bidentate coordination moiety $[V(\eta^2\text{-}CO_2)]^+$ is formed, which lies +47.2 kJ/mol higher in energy than **V-A**. The **V-D** isomer (+47.5 kJ/mol) is a $\eta^1$-OCO weakly solvated structure, in which four $CO_2$ molecules are bound to the $V^+$ cation in the first-coordination shell with an end-on configuration and three $CO_2$ molecules are attached in the second-coordination shell. The **V-E** isomer (+57.6 kJ/mol) features a $\eta^2$-carbonate motif. The **V-F** isomer (+60.5 kJ/mol) contains a $\eta^2$-$O_2C$ motif.

In the **V-B** isomer, the NBO charge of the V atom, oxalate, and $CO_2$ ligands is calculated to be 1.03, −0.74, and 0.71 (Table S2), respectively, implying the charge transfer from the metal to $CO_2$. Natural population analysis analysis shows that the spin population of the V atom and oxalate motif is 1.96 and −0.02, respectively, which indicates that the unpaired electron is mainly located on the V atom. Formally, a doubly charged oxalate-type $C_2O_4^{2-}$ moiety is thus formed in the $[V(CO_2)_7]^+$ cluster, which is different from the singly charged oxalate-type $C_2O_4^-$ moiety reported previously.[32] In the **V-C** isomer ($[V(\eta^2\text{-}CO_2)(CO_2)_6]^+$), the oxidation state of V is +2 and the bent $CO_2$ molecule is determined to be a singly charged $CO_2^-$ anion. The O−C−O bond angle in **V-C** is 141°, which is slightly larger than the value of free $CO_2^-$ anion (134°).[7−12] In the **V-A**, **V-B**, **V-C**, **V-E**, and **V-F** isomers, the $CO_2$ molecule is activated. In contrast, the $CO_2$ molecule is only weakly bound to the metal in the **V-D** isomer.

As shown in Figure 2, the simulated IR spectrum of **V-C** agrees best with the experimental IRPD spectrum. In the simulated IR spectrum of **V-C**, the bands at 2401 and 2373 $cm^{-1}$ are attributed to the in-phase and out-of-phase combinations of $CO_2$ antisymmetric stretches, respectively, which are consistent with the experimental values of bands A (2402 $cm^{-1}$) and B (2376 $cm^{-1}$) (Table 1). The band at 2357 $cm^{-1}$ is due to the antisymmetric stretch of the second-sphere $CO_2$, which reproduces the experimental band C (2348 $cm^{-1}$). The band at 1829 $cm^{-1}$ is assigned to the C═O antisymmetric stretch of $CO_2^-$, which matches the experimental band D (1800 $cm^{-1}$). The band at 1337 $cm^{-1}$ is due to the $CO_2$ symmetric stretch, which is sharply observed at 1363 $cm^{-1}$ (band E) in the IRPD experiment. The band at 1154 $cm^{-1}$ is due to the C═O symmetric stretch of $CO_2^-$, which reproduces the experimental band G (1140 $cm^{-1}$). The bands at 639 and 721 $cm^{-1}$ are attributed to the $CO_2$ bending mode, which matches the experimental bands H (637 and 664 $cm^{-1}$). The experimental band F (1237 and 1267 $cm^{-1}$) is assigned to the overtone of $CO_2$ bending mode as reported previously.[32] The experimental band at 3008 $cm^{-1}$ could be due to the $\nu_1 + \nu_3$ combination of both CO stretching modes of $CO_2^-$.[8] This has also been observed in Al−$CO_2$ complexes.[39]

In the simulated IR spectrum of **V-A** (Figure 2 and Table S3), the peaks at 1022 and 2184 $cm^{-1}$ are due to the V−O and C−O stretches in the $[OVCO]^+$ ion core, respectively, which are not observed experimentally. It thus appears that isomer **V-A** does not contribute to the experimental spectrum. The presence of isomer **V-B** could be eliminated on the basis of experimental absence of the V−O symmetric and antisymmetric stretches of $[V(C_2O_4)]^+$ at 787 and 846 $cm^{-1}$ (Figure 2 and Table S4). The IR spectrum of **V-D** reproduces the experimental bands A−C, E, and H (Figure 2 and Table S5). In the simulated IR spectrum of **V-E** (Figure 2 and Table S6), the peaks at 776, 854, 1066, and 2322 $cm^{-1}$ are absent in the experimental spectrum. For isomer **V-F**, the bending mode of $\eta^2$-$O_2C$ motif (796 $cm^{-1}$) is predicted which is not seen in the experimental spectrum (Figure 2 and Table S7). Thus, we conclude that isomer **V-C** is probably the main isomer present in the experiment. The minor contribution of isomer **V-D**


DOI: 10.1021/acs.jpca.9b00041
J. Phys. Chem. A 2019, 123, 3703−3708

cannot be ruled out because its spectrum matches to the part of the experimental spectrum. As illustrated in Figure 1, different structural motifs yielded characteristic vibrational features in the predicted IR spectra, which might be helpful for structural identification.

It has been reported that the most stable isomer of $[V(CO_2)]^+$ has the end-on configuration, and the high-barrier hinds the transform from weakly solvated structure to oxide-carbonyl structure.[40] Even though **V-A** (oxide-carbonyl structure) is energetically more stable than **V-D** (weakly solvated structure) by 47.5 kJ/mol, the transform from **V-D** to **V-A** could be dynamically prohibitive, resulting in the experimental absence of **V-D**. As aforementioned analysis, one electron is required to be transferred from V to form the doubly charged oxalate-type $C_2O_4^{2-}$ moiety in **V-B**. The experimental absence of **V-B** implies that these charge-transfer processes could be not readily to occur. The barrier for the isomerization from **V-C** to **V-A** and that from **V-C** to **V-B** is calculated to be 69.2 and 34.1 kJ/mol, respectively, suggesting that the **V-C** isomer could be kinetically trapped in the observed structure. It is reminiscent of experimental observations of higher energy isomers on the potential energy surface of charged species.[23,41−45]

**3.2. $[Cr(CO_2)_7]^+$ and $[Mn(CO_2)_7]^+$.** For $[Cr(CO_2)_7]^+$, the most stable isomer, labeled **Cr-D**, is the $\eta^1$-OCO structure (Figure 1). The relative stability of other five structural motifs follows the order of $\eta^2$-$CO_2$ (**Cr-C**) > $\eta^2$-carbonate (**Cr-E**) > $\eta^2$-oxalate (**Cr-B**) > $\eta^2$-$O_2C$ (**Cr-F**) > oxide-carbonyl (**Cr-A**). For $[Mn(CO_2)_7]^+$, the relative stability of the six isomers is in the order of $\eta^1$-OCO (**Mn-D**) > $\eta^2$-$CO_2$ (**Mn-C**) > $\eta^2$-$O_2C$ (**Mn-F**) > oxide-carbonyl (**Mn-A**) > $\eta^2$-carbonate (**Mn-E**) > $\eta^2$-oxalate (**Mn-B**).

In the reaction of a single $CO_2$ molecule with 3d transition-metal cations $M^+$, it has been found that the oxygen-atom transfer can only be achieved by $Sc^+$ and $Ti^+$ via the formation of the oxide-carbonyl structure $[OM(CO)]^+$.[28] Recent experimental IRPD spectra of a series of $[V(CO_2)_n]^+$ clusters exhibited new vibrational features at $n = 7$,[32] which is identified to be a bent $CO_2^-$ species from the present calculations, indicating the ligand-induced activation of $CO_2$. It can be seen from Figure 1 that the most stable isomers of $[Cr(CO_2)_7]^+$ and $[Mn(CO_2)_7]^+$ are the weakly solvated structures, the feature of which is quite different from $[V(CO_2)_7]^+$. IRPD spectroscopy of $[M(CO_2)_n]^+$ (M = Fe, Co, and Cu) indicated that $CO_2$ is weakly bound to the metal cations.[26,27,46] IR spectra of larger $[Ni(CO_2)_n]^+$ clusters provide evidence for the formation of oxide-carbonyl species assisted by solvation.[31]

The calculated IR spectrum of the **Cr-A** isomer for $[Cr(CO_2)_7]^+$ (Figure 3) is similar to that of **V-A** for $[V(CO_2)_7]^+$ (Figure 2). Similar results have also been obtained for other isomers of $[Cr(CO_2)_7]^+$ and $[Mn(CO_2)_7]^+$ (Figures 3 and 4). It can be seen that the predicted IR spectra of different type structures for the $[Cr(CO_2)_7]^+$ and $[Mn(CO_2)_7]^+$ clusters are different in the 800−2300 $cm^{-1}$ region. The IR spectra of $[Cr(CO_2)_7]^+$ and $[Mn(CO_2)_7]^+$ could be measured by the IRPD technique, which helps to identify the structures and shed light on the microscopic mechanism of $CO_2$-metal interactions.

**3.3. Bonding Analysis of Isomer V-C for $[V(CO_2)_7]^+$.** The origin of the ligand-induced activation of $CO_2$ was analyzed using the EDA-NOCV method. Table S8 shows the numerical results for the **V-C** isomer of $[V(CO_2)_7]^+$. The contribution of the orbital interaction $\Delta E_{orb}$ (65.7%) is larger than the electrostatic attraction $\Delta E_{elstat}$ (30.9%). There are two major contributions to the orbital interactions of the bent $CO_2^-$. The associated deformation densities $\Delta\rho_1$ and $\Delta\rho_2$ for the **V-C** isomer is depicted in Figure 5. The direction of the charge migration is red → blue. It becomes obvious that $\Delta E_{orb1}$ comes from the backdonation $[V(CO_2)_6]^+ \rightarrow \pi^*$ antibonding orbital of CO in the bent $CO_2^-$ ligand while $\Delta E_{orb2}$ comes from the weaker donation $[V(CO_2)_6]^+ \leftarrow \pi$ bonding orbital. Both orbital interactions will give rise to the activation of the $CO_2$ ligand. These findings provide physical insights into the fundamental mechanism for $CO_2$ activation on the transition metals, which would have important implications for the rational design of single-atom catalysts.

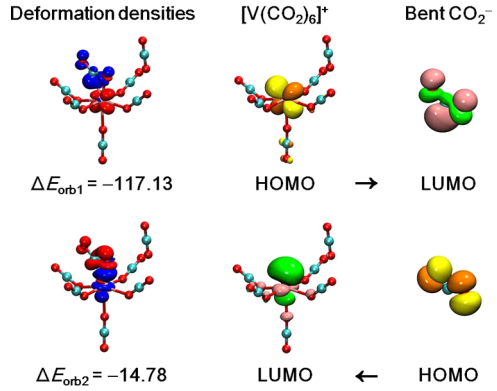


**Figure 5.** Plot of the deformation densities ($\Delta\rho$) of the pairwise orbital interactions between $[V(CO_2)_6]^+$ and the bent $CO_2^-$ ligand in the **V-C** isomer of $[V(CO_2)_7]^+$ and associated stabilization energies $\Delta E$ (kcal/mol) and the shape of the most important interacting orbitals of $[V(CO_2)_6]^+$ and the bent $CO_2^-$ moieties. The color code of the charge flow is red → blue.

## 4. CONCLUSIONS

The interactions of the $CO_2$ molecules with the $V^+$, $Cr^+$, and $Mn^+$ cations were investigated by quantum chemical calculations. The comparison of calculated infrared spectra of $[V(CO_2)_7]^+$ with the experimental infrared spectra revealed the formation of a bent $CO_2^-$ species, indicating the ligand-induced activation of $CO_2$. The most stable isomers of $[Cr(CO_2)_7]^+$ and $[Mn(CO_2)_7]^+$ are the weakly solvated structures, the feature of which is different from $[V(CO_2)_7]^+$. The simulated IR spectra of different type structures for $[Cr(CO_2)_7]^+$ and $[Mn(CO_2)_7]^+$ are different in the 800−2300 $cm^{-1}$ region, which could be measured by the IRPD technique and thus helps to identify the structures.

## ■ ASSOCIATED CONTENT

### Supporting Information

The Supporting Information is available free of charge on the ACS Publications website at DOI: 10.1021/acs.jpca.9b00041.

Relative energies of the isomers with different spin states for $[V(CO_2)_7]^+$, NBO charges of $[M(CO_2)_7]^+$ (M = V, Cr, and Mn), calculated harmonic frequencies and band assignments of the **V-A**, **V-B**, **V-D**, **V-E**, and **V-F** isomers for $[V(CO_2)_7]^+$, and EDA-NOCV results of the **V-C** isomers for $[V(CO_2)_7]^+$ (PDF)



DOI: 10.1021/acs.jpca.9b00041
J. Phys. Chem. A 2019, 123, 3703−3708

## AUTHOR INFORMATION


### Corresponding Author

*E-mail: ljiang@dicp.ac.cn. Phone: +86-411-84379857. Fax: +86-411-84675584.

### ORCID

Hua Xie: 0000-0003-2091-6457

Ling Jiang: 0000-0002-8485-8893

### Author Contributions

§D.Y. and X.K. contributed equally to this work.


### Notes

The authors declare no competing financial interest.

## ACKNOWLEDGMENTS

The authors thank Professor Zhiling Liu for helpful discussions. This work was supported by the National Natural Science Foundation of China (grant nos. 21327901, 21503222, 21673231, 21673234, and 21688102), the Strategic Priority Research Program of the Chinese Academy of Sciences (CAS) (grant no. XDB17000000), Dalian Institute of Chemical Physics (DICP DCLS201702), and Dalian National Laboratory for Clean Energy (DNL), CAS, and K. C. Wong Education Foundation.

## REFERENCES


(1) Gibson, D. H. The Organometallic Chemistry of Carbon Dioxide. *Chem. Rev.* **1996**, *96*, 2063−2096.

(2) Taifan, W.; Boily, J.-F.; Baltrusaitis, J. Surface Chemistry of Carbon Dioxide Revisited. *Surf. Sci. Rep.* **2016**, *71*, 595−671.

(3) Walker, N. R.; Walters, R. S.; Duncan, M. A. Frontiers in the Infrared Spectroscopy of Gas Phase Metal Ion Complexes. *New J. Chem.* **2005**, *29*, 1495−1503.

(4) Weber, J. M. The Interaction of Negative Charge with Carbon Dioxide - Insight into Solvation, Speciation and Reductive Activation from Cluster Studies. *Int. Rev. Phys. Chem.* **2014**, *33*, 489−519.

(5) Schwarz, H. Metal-mediated Activation of Carbon Dioxide in the Gas Phase: Mechanistic Insight Derived from a Combined Experimental/Computational Approach. *Coord. Chem. Rev.* **2017**, *334*, 112−123.

(6) Dodson, L. G.; Thompson, M. C.; Weber, J. M. Characterization of Intermediate Oxidation States in $CO_2$ Activation. *Annu. Rev. Phys. Chem.* **2018**, *69*, 231−252.

(7) Zhou, M.; Andrews, L. Infrared Spectra of the $CO_2^-$ and $C_2O_4^-$ Anions Isolated in Solid Argon. *J. Chem. Phys.* **1999**, *110*, 2414−2422.

(8) Thompson, W. E.; Jacox, M. E. The Vibrational Spectra of $CO_2^+$, $(CO_2)_2^+$, $CO_2^-$, and $(CO_2)_2^-$ Trapped in Solid Neon. *J. Chem. Phys.* **1999**, *111*, 4487−4496.

(9) Hartman, K. O.; Hisatsune, I. C. Infrared Spectrum of Carbon Dioxide Anion Radical. *J. Chem. Phys.* **1966**, *44*, 1913−1918.

(10) Ovenall, D. W.; Whiffen, D. H. Electron Spin Resonance and Structure of the $CO_2^-$ Radical Ion. *Mol. Phys.* **1961**, *4*, 135−144.

(11) Sommerfeld, T.; Meyer, H.-D.; Cederbaum, L. S. Potential Energy Surface of the $CO_2^-$ Anion. *Phys. Chem. Chem. Phys.* **2004**, *6*, 42−45.

(12) Gutsev, G. L.; Bartlett, R. J.; Compton, R. N. Electron Affinities of $CO_2$, OCS, and $CS_2$. *J. Chem. Phys.* **1998**, *108*, 6756−6762.

(13) Thompson, M. C.; Ramsay, J.; Weber, J. M. Solvent-Driven Reductive Activation of $CO_2$ by Bismuth: Switching from Metalloformate Complexes to Oxalate Products. *Angew. Chem., Int. Ed.* **2016**, *55*, 15171−15174.

(14) Knurr, B. J.; Weber, J. M. Structural Diversity of Copper-$CO_2$ Complexes: Infrared Spectra and Structures of $Cu(CO_2)_n^-$ Clusters. *J. Phys. Chem. A* **2014**, *118*, 10246−10251.

(15) Knurr, B. J.; Weber, J. M. Solvent-Mediated Reduction of Carbon Dioxide in Anionic Complexes with Silver Atoms. *J. Phys. Chem. A* **2013**, *117*, 10764−10771.

(16) Knurr, B. J.; Weber, J. M. Solvent-Driven Reductive Activation of Carbon Dioxide by Gold Anions. *J. Am. Chem. Soc.* **2012**, *134*, 18804−18808.

(17) Knurr, B. J.; Weber, J. M. Infrared Spectra and Structures of Anionic Complexes of Cobalt with Carbon Dioxide Ligands. *J. Phys. Chem. A* **2014**, *118*, 4056−4062.

(18) Knurr, B. J.; Weber, J. M. Interaction of Nickel with Carbon Dioxide in $Ni(CO_2)_n^-$ Clusters Studied by Infrared Spectroscopy. *J. Phys. Chem. A* **2014**, *118*, 8753−8757.

(19) Miller, G. B. S.; Esser, T. K.; Knorke, H.; Gewinner, S.; Schöllkopf, W.; Heine, N.; Asmis, K. R.; Uggerud, E. Spectroscopic Identification of a Bidentate Binding Motif in the Anionic Magnesium-$CO_2$ Complex ($ClMgCO_2^-$). *Angew. Chem., Int. Ed.* **2014**, *53*, 14407−14410.

(20) Thompson, M. C.; Dodson, L. G.; Weber, J. M. Structural Motifs of $Fe(CO_2)_n^-$ Clusters ($n$ = 3-7). *J. Phys. Chem. A* **2017**, *121*, 4132−4138.

(21) Dodson, L. G.; Thompson, M. C.; Weber, J. M. Titanium Insertion into CO Bonds in Anionic Ti-$CO_2$ Complexes. *J. Phys. Chem. A* **2018**, *122*, 2983−2991.

(22) Yanagimachi, A.; Koyasu, K.; Valdivielso, D. Y.; Gewinner, S.; Schöllkopf, W.; Fielicke, A.; Tsukuda, T. Size-Specific, Dissociative Activation of Carbon Dioxide by Cobalt Cluster Anions. *J. Phys. Chem. C* **2016**, *120*, 14209−14215.

(23) Green, A. E.; Justen, J.; Schöllkopf, W.; Gentleman, A. S.; Fielicke, A.; Mackenzie, S. R. IR Signature of Size-Selective $CO_2$ Activation on Small Platinum Cluster Anions, $Pt_n^-$ ($n$ = 4-7). *Angew. Chem., Int. Ed.* **2018**, *57*, 14822−14826.

(24) Armentrout, P. B.; Koizumi, H.; MacKenna, M. Sequential Bond Energies of $Fe^+(CO_2)_n$, $n$=1-5, Determined by Threshold Collision-Induced Dissociation and Ab Initio Theory. *J. Phys. Chem. A* **2005**, *109*, 11365−11375.

(25) Walters, R. S.; Brinkmann, N. R.; Schaefer, H. F.; Duncan, M. A. Infrared Photodissociation Spectroscopy of Mass-selected $Al^+(CO_2)_n$ and $Al^+(CO_2)_nAr$ Clusters. *J. Phys. Chem. A* **2003**, *107*, 7396−7405.

(26) Iskra, A.; Gentleman, A. S.; Kartouzian, A.; Kent, M. J.; Sharp, A. P.; Mackenzie, S. R. Infrared Spectroscopy of Gas-Phase $M^+(CO_2)_n$ ($M$ = Co, Rh, Ir) Ion-Molecule Complexes. *J. Phys. Chem. A* **2017**, *121*, 133−140.

(27) Zhao, Z.; Kong, X.; Yang, D.; Yuan, Q.; Xie, H.; Fan, H.; Zhao, J.; Jiang, L. Reactions of Copper and Silver Cations with Carbon Dioxide: An Infrared Photodissociation Spectroscopic and Theoretical Study. *J. Phys. Chem. A* **2017**, *121*, 3220−3226.

(28) Koyanagi, G. K.; Bohme, D. K. Gas-phase Reactions of Carbon Dioxide with Atomic Transition-metal and Main-group Cations: Room-temperature Kinetics and Periodicities in Reactivity. *J. Phys. Chem. A* **2006**, *110*, 1232−1241.

(29) Xing, X.-p.; Wang, G.-j.; Wang, C.-x.; Zhou, M.-f. Infrared Photodissociation Spectroscopy of $Ti^+(CO_2)_2Ar$ and $Ti^+(CO_2)_n$ ($n$=3-7) Complexes. *Chin. J. Chem. Phys.* **2013**, *26*, 687−693.

(30) Jaeger, J. B.; Jaeger, T. D.; Brinkmann, N. R.; Schaefer, H. F.; Duncan, M. A. Infrared Photodissociation Spectroscopy of $Si^+(CO_2)_n$ and $Si^+(CO_2)_nAr$ Complexes - Evidence for Unanticipated Intracluster Reactions. *Can. J. Chem.* **2004**, *82*, 934−946.

(31) Walker, N. R.; Walters, R. S.; Grieves, G. A.; Duncan, M. A. Growth Dynamics and Intracluster Reactions in $Ni^+(CO_2)_n$ Complexes via Infrared Spectroscopy. *J. Chem. Phys.* **2004**, *121*, 10498−10507.

(32) Ricks, A. M.; Brathwaite, A. D.; Duncan, M. A. IR Spectroscopy of Gas Phase $V(CO_2)_n^+$ Clusters: Solvation-Induced Electron Transfer and Activation of $CO_2$. *J. Phys. Chem. A* **2013**, *117*, 11490−11498.

(33) Frisch, M. J. e. a. *Gaussian 09*, Revision D.01; Gaussian, Inc.: Wallingford, CT, USA, 2009.

(34) Jiang, L.; Zhang, X.-B.; Han, S.; Xu, Q. Unique Structural Trends in the Lanthanoid Oxocarbonyl Complexes. *Inorg. Chem.* **2008**, *47*, 4826−4831.




DOI: 10.1021/acs.jpca.9b00041
J. Phys. Chem. A 2019, 123, 3703−3708

(35) Mitoraj, M. P.; Michalak, A.; Ziegler, T. A Combined Charge and Energy Decomposition Scheme for Bond Analysis. *J. Chem. Theory Comput.* **2009**, *5*, 962−975.
(36) te Velde, G.; Bickelhaupt, F. M.; Baerends, E. J.; Fonseca Guerra, C.; Van Gisbergen, S. J. A.; Snijders, J. G.; Ziegler, T. Chemistry with ADF. *J. Comput. Chem.* **2001**, *22*, 931−967.
(37) Guerra, C. F.; Snijders, J. G.; te Velde, G.; Baerends, E. J. Towards an Order-N DFT Method. *Theor. Chem. Acc.* **1998**, *99*, 391−403.
(38) *ADF2018, SCM, Theoretical Chemistry*; Vrije Universiteit: Amsterdam, The Netherlands, 2018. http://www.scm.com.
(39) Le Quere, A. M.; Xu, C.; Manceron, L. Vibrational Spectra, Structures, and Normal-Coordinate Analysis of Al-$CO_2$ Complexes Isolated in Solid Argon. *J. Phys. Chem.* **1991**, *95*, 3031−3037.
(40) Sun, Y.; Sun, X.; Huang, X. Reaction of $CO_2$ with Atomic Transition Metal $M^{+/0/-}$ Ions: A Theoretical Study. *J. Phys. Chem. A* **2018**, *122*, 5848−5860.
(41) Hou, G.-L.; Kong, X.-T.; Valiev, M.; Jiang, L.; Wang, X.-B. Probing the Early Stages of Solvation of cis-Pinate Dianions by Water, Acetonitrile, and Methanol: A Photoelectron Spectroscopy and Theoretical Study. *Phys. Chem. Chem. Phys.* **2016**, *18*, 3628−3637.
(42) Brites, V.; Cimas, A.; Spezia, R.; Sieffert, N.; Lisy, J. M.; Gaigeot, M.-P. Stalking Higher Energy Conformers on the Potential Energy Surface of Charged Species. *J. Chem. Theory Comput.* **2015**, *11*, 871−883.
(43) Yang, B.; Rodgers, M. T. Alkali Metal Cation Binding Affinities of Cytosine in the Gas Phase: Revisited. *Phys. Chem. Chem. Phys.* **2014**, *16*, 16110−16120.
(44) Papadopoulos, G.; Svendsen, A.; Boyarkin, O. V.; Rizzo, T. R. Conformational Distribution of Bradykinin $[bk+2\ H]^{2+}$ Revealed by Cold Ion Spectroscopy Coupled with FAIMS. *J. Am. Soc. Mass Spectrom.* **2012**, *23*, 1173−1181.
(45) Goebbert, D. J.; Wende, T.; Jiang, L.; Meijer, G.; Sanov, A.; Asmis, K. R. IR Spectroscopic Characterization of the Thermally Induced Isomerization in Carbon Disulfide Dimer Anions. *J. Phys. Chem. Lett.* **2010**, *1*, 2465−2469.
(46) Gregoire, G.; Duncan, M. A. Infrared Spectroscopy to Probe Structure and Growth Dynamics in $Fe^+$-$(CO_2)_n$ Clusters. *J. Chem. Phys.* **2002**, *117*, 2120−2130.


DOI: 10.1021/acs.jpca.9b00041
*J. Phys. Chem. A* 2019, 123, 3703−3708